

Factors controlling secondary ice production in cumulus clouds

Yahui Huang,^{a*} Alan M. Blyth,^b Philip R. A. Brown,^c Tom W. Choularton^d and Zhiqiang Cui^a

^a*School of Earth and Environment, Institute for Climate and Atmospheric Science, University of Leeds, UK*

^b*National Centre for Atmospheric Science, School of Earth and Environment, University of Leeds, UK*

^c*Met Office, Exeter, UK*

^d*School of Earth, Atmospheric and Environmental Sciences, University of Manchester, UK*

*Correspondence to: Y. Huang, School of Earth and Environment, University of Leeds, LS2 9JT, UK. E-mail: y.huang@leeds.ac.uk

Aircraft measurements of two cumulus clouds were made during the Ice and Precipitation Initiation in Cumulus campaign over the British Isles. The 18 May 2006 cloud had high concentrations of ice particles and conditions were conducive for the Hallett–Mossop (HM) process of secondary ice production, but the 13 July 2005 cloud had low concentrations. A bin-resolved cloud model was used to investigate several factors that are known to control the HM process using the observations of the two clouds. For the 2006 cloud, the model results show that the fast production of graupel by directly freezing of supercooled raindrops through collisional collection with ice particles was crucial to the activation of the HM process. Switching off raindrop freezing led to much delayed and suppressed formation of graupel particles, and hence a negligible HM process. Sensitivity studies were performed on the concentration of primary ice particles required to kick-start the HM process. It was found that a concentration of the first ice as low as 0.01 L^{-1} could be sufficient, as long as there was a large enough concentration of cloud droplets (small and large) available when a significant number of graupel particles developed in the HM temperature zone. For the modelled 2005 cloud, the HM process did not operate effectively mainly because of the low concentration of supercooled raindrops and hence graupel. The HM process was also hindered by the relatively greater number of aerosols, and higher temperatures at cloud base and top.

Key Words: ice multiplication; primary ice; supercooled raindrops; droplet spectrum; aerosol; cumulus clouds

Received 18 December 2015; Revised 7 December 2016; Accepted 14 December 2016; Published online in Wiley Online Library 14 February 2017

1. Introduction

Ice plays an important role in global rainfall (Field and Heymsfield, 2015). Therefore it is important to understand the microphysical processes involved in the formation and development of ice particles and precipitation in order to improve numerical weather prediction and global climate models.

There have been many reports of ice particle concentrations that are much higher than typical concentrations of ice nuclei (e.g. Mossop *et al.*, 1972; Hobbs and Rangno, 1985; Harris-Hobbs and Cooper, 1987; Blyth and Latham, 1993; Bower *et al.*, 1996). Several secondary ice production processes are suggested to be responsible, but the Hallett–Mossop (HM) process of splintering during riming (Hallett and Mossop, 1974) is the most studied and the most quantified. Although the conditions for the operation of the HM process are strict, there is considerable evidence that this process operates in cumulus clouds in many parts of the world (e.g. Harris-Hobbs and Cooper, 1987; Blyth

and Latham, 1993; Huang *et al.*, 2008; Crosier *et al.*, 2011). Results of calculations performed by Chisnell and Latham (1976) showed that supercooled raindrops can play an important role in the glaciation of clouds by the HM rime-splinter mechanism because instant rimers are produced when the raindrops freeze. Later modelling studies by, for example, Koenig (1977), Lamb *et al.* (1981), Phillips *et al.* (2001), Sun *et al.* (2012) and Crawford *et al.* (2012) further illustrated the importance of supercooled raindrops in the HM multiplication process. In addition, Chisnell and Latham (1976) found that the rate of glaciation may be substantially enhanced if the raindrops themselves produced splinters as they froze. Supercooled raindrops have been observed in convective clouds, for example in Florida by Bringi *et al.* (1997), in New Mexico by Blyth *et al.* (1997) and in England by Caylor and Illingworth (1987).

The study of Hallett and Mossop (1974) demonstrated that the secondary ice crystals were produced in the laboratory by a riming rod that reproduced the growth of graupel particles by riming. Mossop and Hallett (1974) found that the splinter production

rate is directly proportional to the concentration of droplets with $d > 23 \mu\text{m}$. Mossop (1978a) performed further experiments which also show the importance of the small-drop end of the cloud droplet spectrum in the splintering process and produced a formula that is a best fit to the data. However, the nature of the splintering process is not yet clear. By reviewing the work on the ice multiplication processes and the nature of the splinter production in particular, Mossop (1985) pointed out that there has been 'strong evidence that the production of ice splinters during riming is associated with the build-up of pressure within freezing drops', but the spike formation upon shattering is the subject of some discussion. Alternative processes are possible (e.g. Knight, 2012). In this article, we present model analysis based on two very different convective cloud cases; one with high and the other with low concentration of ice particles. The purpose is to determine the importance of supercooled raindrops in single-thermal, relatively short-lived clouds and the concentration of ice crystals produced by primary ice nucleation required to allow the HM process (as currently understood) to operate efficiently. The clouds in the two cases were observed with the Facility for Airborne Atmospheric Measurements (FAAM) BAe-146 research aircraft during the Ice and Precipitation Initiation in Cumulus (ICEPIC) campaign in southwest England and Wales in the summer of 2005 and May 2006. Modelling studies were performed using a detailed bin microphysics model. The observations are briefly described in section 2. The instruments and the cloud model are introduced in sections 2 and 3, respectively. The results of simulations are presented in section 4. Summary and conclusions are given in section 5.

2. Overview of the observational cases

The ICEPIC field campaign was conducted in southwest England during 2005–2006 with the goal of understanding and quantifying the formation and growth of ice particles in cumulus congestus clouds with the BAe-146 research aircraft.

Microphysics instruments on board the aircraft included the Fast Forward Scattering Spectrometer Probe (FFSSP), the 2DC (cloud) and 2DP (precipitation) probes (Brenquier *et al.*, 1998; Jensen and Granek, 2002; Knollenberg, 1970; Korolev, 2007), and the Cloud Particle Imager (CPI; Lawson *et al.*, 2001). The liquid water content (LWC) was measured with the Johnson–Williams probe (Strapp *et al.*, 2003). Aerosol concentration and size distribution were measured with the Passive Cavity Aerosol Spectrometer Probe (PCASP; Strapp *et al.*, 1992). Huang *et al.* (2008) gives further details of the instruments. In this article two contrasting cases are studied, Case A on 18 May 2006 and Case B on 13 July 2005. Details of the cases can be found in Huang (2014, Chapter 5) and only an overview is given here.

Aircraft penetrations in Case A were made through convection along a weak convergence line over the peninsula of southwest England. Cloud tops reached the height where the temperatures were approximately -18°C from the MSG IR-derived cloud-top temperature. Case B was under the influence of a weak high pressure ridge over Wales and England. Penetrations

were through isolated convection. Some clouds near the Chilbolton 3 GHz radar reached an altitude of about 6 km ($T \approx -12^\circ\text{C}$).

Table 1 summarizes the cloud properties measured by the instruments on board the aircraft. Although the maximum vertical velocities of the two cases were comparable, Case B had about 1.4 times higher concentration of cloud droplets than Case A. However, the maximum number concentration of ice particles, estimated with the concentration of particles larger than $150 \mu\text{m}$ from the 2DC and 2DP, and the maximum concentration of cloud particles larger than 1 mm were very different in the two cases. The threshold of $150 \mu\text{m}$ was used based on visual inspection of the 2D images to reduce the impact of possible artifacts such as shattering on the concentration of small ice particles (Huang *et al.*, 2008; Korolev, 2010).

During the third penetration in Case A at $z \approx 2.7 \text{ km}$ ($T \approx -4.5^\circ\text{C}$, $T_{\text{ct}} \approx -10^\circ\text{C}$), the ice concentration reached a maximum value of 110 L^{-1} , which is greater than the typical ice concentration due to primary nucleation estimated by the formula of Meyers *et al.* (1992) with the cloud-top temperature T_{ct} of about -10°C . The conditions for secondary ice production by the HM process were met in this case. In contrast, the maximum ice particle concentration in Case B was about 6 L^{-1} . The observations suggested that the HM process may have operated in the clouds observed in Case A, but not in those observed in Case B. Supercooled raindrops were observed in both cases, but the concentration was greater in Case A. Modelling studies using the Model of Aerosol and Chemistry in Convective Clouds (MAC3) were performed in order to investigate the role of supercooled raindrops in the formation of ice particles and the multiplication due to the HM process. No other secondary ice process was investigated.

3. Model and set-up

3.1. The model

MAC3 is an axisymmetric model with bin-resolved microphysics for drop, ice crystal, graupel and snow, and aerosol. The liquid microphysical processes include activation of cloud condensation nuclei (CCN), diffusional growth, collision–coalescence, break-up, evaporation. The primary ice processes have immersion freezing (Bigg, 1953), deposition/condensation freezing (Meyers *et al.*, 1992), and contact freezing (Meyers *et al.*, 1992; Cotton *et al.*, 1986). For the secondary ice production process, only the HM process of splintering during riming is considered in the model. The formula used is given by Mossop (1978a), where the splinter production rate is proportional to the concentration of large ($d > 24 \mu\text{m}$) and small ($d < 13 \mu\text{m}$) droplets swept by graupel particles in the HM temperature zone per second. There are many other microphysical processes included. A detailed description of the model can be found in Tzivion *et al.* (1987), Reisin *et al.* (1996) and Yin *et al.* (2005). The model has been previously used extensively (e.g. Cui and Carslaw, 2006; Cui *et al.*, 2006, 2011; Huang *et al.*, 2008, 2011; Blyth *et al.*, 2012).

Table 1. Summary of observations for Case A (18 May 2006) and Case B (13 July 2005).

Variable	Description	Case A	Case B
w (m s^{-1})	Vertical velocity	12	13
N_d (cm^{-3})	Droplet concentration from FFSSP	170	240
N_c (L^{-1})	Cloud particle concentration from 2DC	4524	360
N_p (m^{-3})	Cloud particle concentration from 2DP	65000	2200
		8 (Run 1)	0.2 (Run 1)
N_{150} (L^{-1})	Concentration from 2DC/2DP for $d > 150 \mu\text{m}$	110 (Run 3)	6 (Run 3)
		200 (Run 1)	6 (Run 1)
$N_{1\text{mm}}$ (m^{-3})	Concentration from 2DP for $d > 1 \text{ mm}$	1200 (Run 3)	100 (Run 3)

Maximum values are shown.

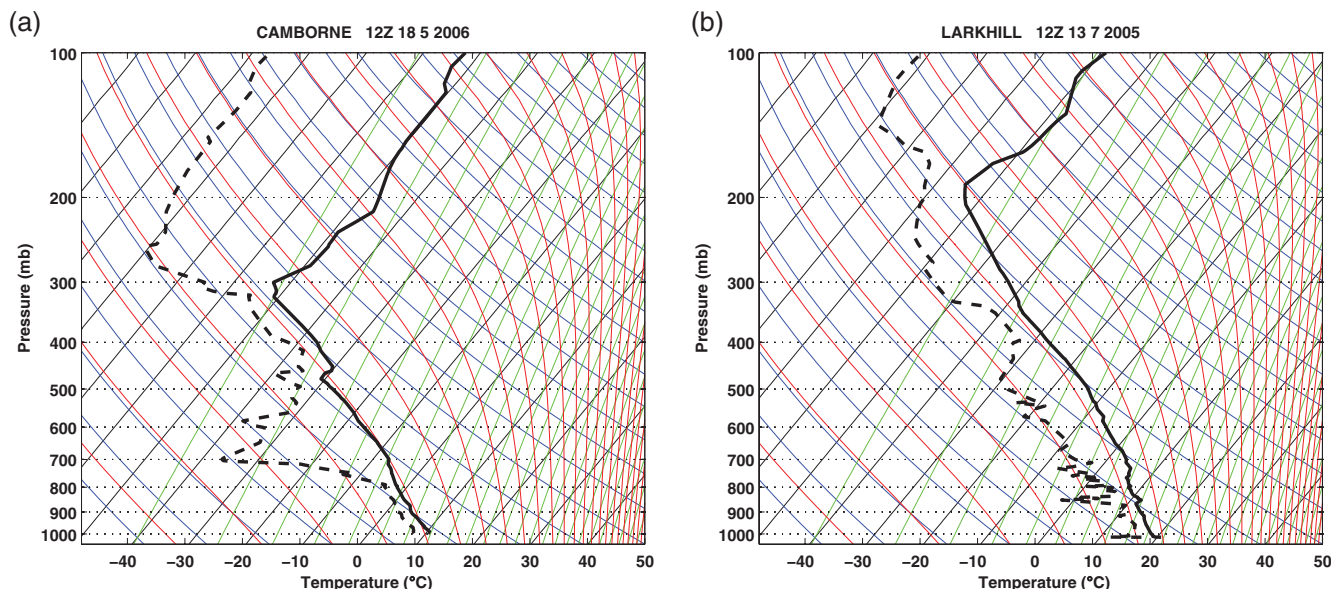


Figure 1. Soundings used for the simulations of (a) Case A and (b) Case B. [Colour figure can be viewed at wileyonlinelibrary.com].

Table 2. Background aerosol properties (N_a ; cm^{-3}) used for Case A (18 May 2006) and Case B (13 July 2005).

Category	A	B
Small ($0.06 < d < 0.2 \mu\text{m}$)	207.78	520.28
Large ($0.2 < d < 2 \mu\text{m}$)	42.79	389.56
Giant ($2 < d < 20 \mu\text{m}$)	0.82	0.31
Total ($0.002 < d < 40 \mu\text{m}$)	561.00	1219.00

Table 3. Description of the simulations.

Run	Description
S10	For Case A: modified Camborne sounding at 1200 UTC 18 May 2006; $N_a = 561 \text{ cm}^{-3}$; initial thermal bubble = 0.9 K at $m = 3$ and $k = 2$ to 5
S11	As S10 but no raindrops collecting ice or snow to become graupel and no immersion freezing to graupel
S12	As S10 but no immersion freezing
S13	As S10 but no deposition/condensation freezing
S14	As S12 but with 0.5% of deposition/condensation freezing
S15	As S12 but with 0.05% of deposition/condensation freezing
S20	For Case B: Larkhill sounding at 1200 UTC 13 July 2005; $N_a = 1219 \text{ cm}^{-3}$; initial thermal bubble = 0.9 K at $m = 3$ and $k = 2-3$
S21	As S20 but using aerosol data for Case A with $N_a = 561 \text{ cm}^{-3}$
S22	As S21 but using initial thermal bubble = 1.5 K at $m = 2-3$ and $k = 2-3$
S23	As S22 but using enhanced deposition/condensation freezing scheme by twofold and no restriction of $T < -5^\circ\text{C}$

3.2. Set-up of simulations

The model domain used was 12 km in the vertical and 6 km in the radial direction with a grid size of 300 and 150 m, respectively, for both cases. The sounding (Figure 1) used in the Case A simulation was made at Camborne at 1200 UTC. It was modified at levels from 0.3 to 6 km by using the data from the aircraft profile flight around this area at about 1015 UTC. For the simulations of Case B, a slightly modified sounding (with the lapse rate set to $0.01^\circ\text{C m}^{-1}$ only at low levels) from Larkhill at 1200 UTC was used for the background conditions. For each case, the observations of aerosol particle distribution from the PCASP in the sub-cloud layer were used for the aerosol background conditions by using the same approach as in Huang *et al.* (2008). Table 2 shows the background aerosol properties used for the simulations. To investigate the role of supercooled raindrops in the formation and development of ice particles, sensitivity tests were conducted for both cases. Table 3 gives the description of the simulations. S10 to S15 are the simulations of Case A and S20 to S23 of Case B. S10 and S20 are the respective reference runs.

4. Results

4.1. Reference Run S10: the 18 May 2006 cloud

Run S10 was made using the observed background aerosol distribution given in Table 2. Figure 2 shows a time sequence of vertical sections with the spatial distribution of the wind field and concentrations of drops, ice and graupel particles from 15 to 40 min into the simulation at 5 min intervals.

The cloud was in a development stage before 25 min (Figures 2(a)–(c)). The maximum vertical velocity and concentration of cloud drops at 2.1 km were about 7 m s^{-1} and 149 cm^{-3} , respectively, in agreement with the observations. Primary ice nucleation occurred at the cloud top ($T \approx -6^\circ\text{C}$), where the deposition/condensation freezing process dominated.

m and k are the grid index in the vertical and radial directions, respectively.

There was no significant production of graupel particles at this time. At 30 min into the simulation (Figure 2(d)), the maximum vertical velocity increased to about 11 m s^{-1} at 3 km. Meanwhile, the concentration of graupel particles produced by the model had increased significantly ($> 0.1 \text{ L}^{-1}$) in the HM zone in a place with weak updraughts. This allowed the process of ice splintering during riming to operate effectively. The maximum ice production rate of the HM process was $1075 \text{ m}^{-3} \text{ s}^{-1}$ at 30 min. Two minutes later, the ice concentration reached a cloud maximum of 170.8 L^{-1} at $z \approx 3 \text{ km}$ and $x \approx 0.75 \text{ km}$ in the HM zone (-3 to -8°C). The maximum ice concentration in the HM temperature range was 83.47 L^{-1} at 35 min (Figure 2(e)). At 40 min into the simulation (Figure 2(f)) the cloud started to glaciate and the maximum concentration of drops was only 47 cm^{-3} . The main features, such as the maximum vertical velocity, the maximum concentration of drops, and the maximum concentration of ice particles, of the simulated cloud are in reasonable agreement with the observations.

The HM process is responsible for the high concentrations of ice particles in the model reference run. The agreement of model parameters with the observations suggests that the observed high concentrations of ice particles are a result of the HM process, although it is possible that a different process not included in the model was responsible. The timing of the appearance of significant amount of graupel in the HM temperature zone is crucial to the effective operation of the HM process since there would not be sufficient number of droplets available in these

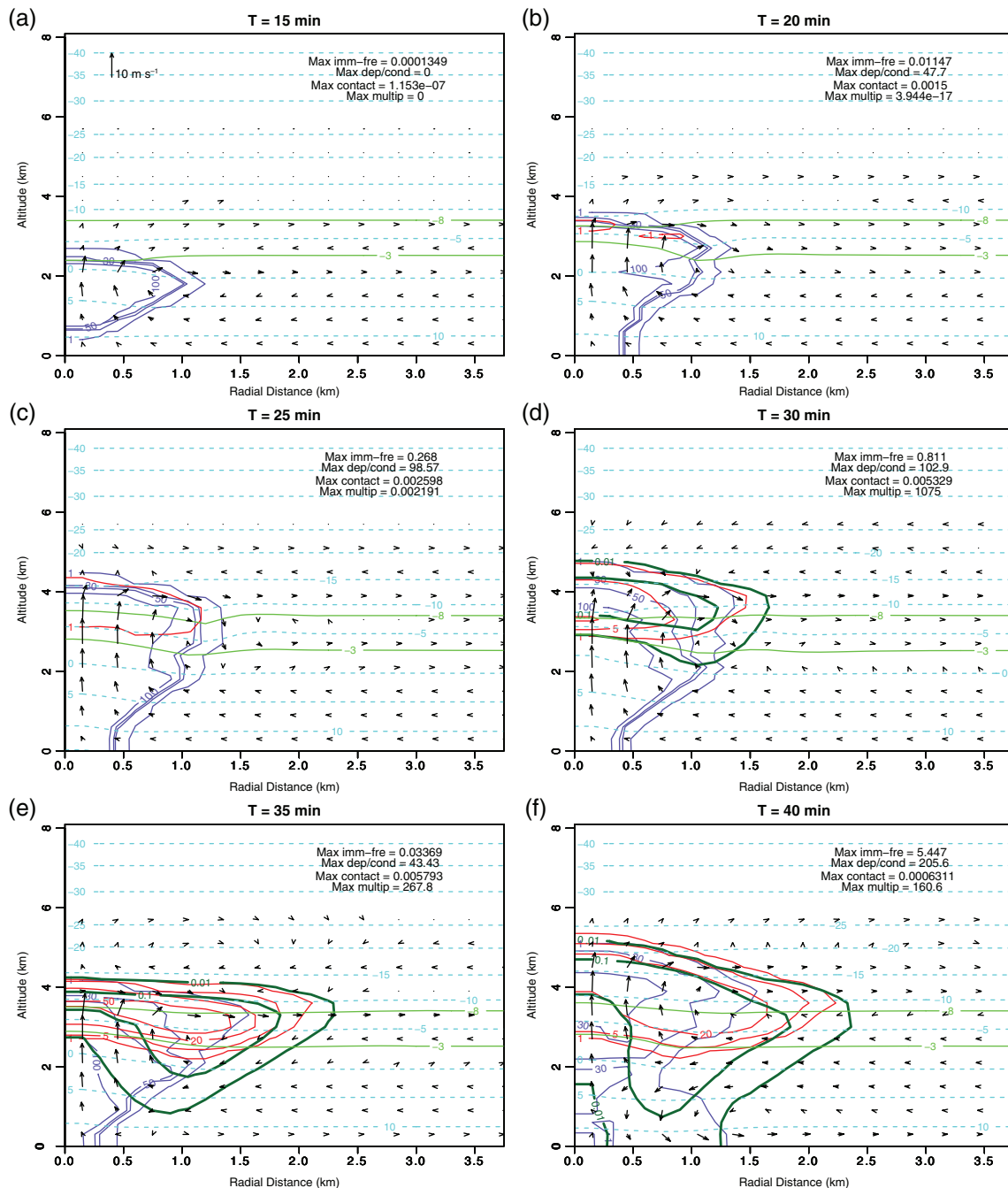


Figure 2. Time sequence for the reference run S10 of spatial distribution of wind vectors, concentration of drops, ice crystals, and graupel particles at (a) 15 min, (b) 20 min, (c) 25 min, (d) 30 min, (e) 35 min and (f) 40 min. The blue lines are the concentration of drops with contours at 1, 30, 50, 100, 300 cm⁻³. The red lines are the concentration of ice crystals with contours at 1, 5, 20, 50, 100 L⁻¹. The green lines are the concentration of graupel particles with contours at 0.01, 0.1, 1 L⁻¹. The dashed lines are isotherms in °C. The maximum ice production rates are also shown in each panel in m⁻³ s⁻¹. The scale for the vectors is shown in (a).

short-lived clouds if the graupel fell into the HM zone after developing above it. Graupel particles can be generated by the depositional growth of ice particles followed by riming, or by short-circuiting that process by direct freezing of supercooled raindrops through immersion freezing or through collisional collection with ice crystals. Some modelling studies (e.g. Chisnell and Latham, 1976; Phillips *et al.*, 2001; Huang *et al.*, 2008) have shown the importance of the presence of supercooled raindrops to the development of ice particles in the clouds. The observations in the 18 May case presented above showed that supercooled raindrops were present in the cloud at $z \approx 2.1$ km ($T \approx -1^\circ\text{C}$) (Huang, 2014, Chapter 5). The simulation showed that the supercooled raindrops first appeared at $z \approx 2.1$ km at 25 min into the simulation but formed at upper levels within the HM zone at about 2 min earlier (Figure 3). The concentrations of the raindrops above 3 km reached a maximum before 30 min. Figure 4(a) shows the evolution of the maximum ice mass at levels from $z \approx 2.4$ to 4.2 km. From Figure 4(a), it can be seen that ice

particles first appeared at $z \approx 3$ km ($T \approx -5^\circ\text{C}$) at about 17 min. The production of these ice particles in the model was due to deposition/condensation freezing, since the freezing in Meyers' scheme (Meyers *et al.*, 1992) commences at $T \approx -5^\circ\text{C}$ ($z \approx 3$ km in this case). The ice particles grew quickly at lower temperatures and higher supersaturation with respect to ice at the upper levels. The mass first reached 0.001 g m^{-3} at $z \approx 3.9$ km ($T \approx -12^\circ\text{C}$) at about 25 min and before 26 min the ice mass at the levels from $z \approx 3.3$ to 4.2 km had all increased to 0.001 g m^{-3} . The main mechanism for the freezing of the supercooled raindrops into graupel particles in the model run is by collisional collection of ice particles. For appreciable freezing to occur, the ice crystals need to grow large enough in order for the collection efficiency to increase (Lew and Pruppacher, 1983). The increase in ice mass indicated the growth in size of the ice crystals, because there was no sharp increase in ice concentration until 30 min (Figure 2). Figure 4(b) shows the evolution of the maximum concentration of graupel particles at levels from $z \approx 2.4$ to

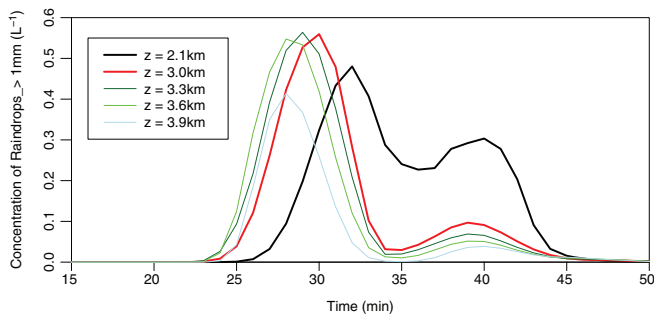


Figure 3. Evolution of maximum concentration of raindrops at $z = 2.1$ to 3.9 km for S10.

4.2 km. The production of graupel started first at $z \approx 3.9$ km ($T \approx -12^\circ\text{C}$) at about 24 min and then a significant amount ($> 0.1 \text{ L}^{-1}$) of graupel was developed at about 27 min at 3.9 km. At 30 min, a significant number (0.1 L^{-1}) of graupel particles developed at 3 km ($T \approx -5^\circ\text{C}$), which allowed the secondary production of ice splinters by riming to commence (Figure 2(d)). Note that it only took about 6 min from the first formation of graupel at 3.9 km to the production of 0.1 L^{-1} of graupel particles at 3 km.

It will be seen in the following sensitivity simulations that the production of graupel was dominated by the freezing of the supercooled raindrops, which occurred rapidly mainly due to the collection of ice crystals by the supercooled raindrops. So it is critical that ice particles are produced at a relatively high temperature of $T \geq -6^\circ\text{C}$.

4.2. Sensitivity simulations S11 to S15: the 18 May 2006 cloud

The sensitivity tests are described in Table 3. The test run S11 was designed to investigate if the mechanism of raindrop freezing dominates the production of graupel, and also the effect on the activation of the HM process. In S11, the production rate of graupel through immersion freezing of raindrops was set to zero and the kernels of raindrops collecting ice and snow were also set to zero. Therefore, the formation of graupel in S11 was only by the depositional growth of ice particles followed by riming, rather than by the freezing of supercooled raindrops. Other conditions remained the same as in the reference run S10. It is evident by comparing Figure 5 with Figure 4 that the formation of graupel in S11 was delayed by about 15 min at $z \approx 3$ km, compared to the reference run. The maximum concentration of graupel in S11 was also much less than in the reference run. The delayed and suppressed production of graupel had a great impact on the operation of the HM process. The results are shown in Table 4. The maximum ice production rate due to the HM process was only $2 \times 10^{-4} \text{ m}^{-3} \text{ s}^{-1}$ which occurred at 45 min. There was no effective operation of the HM process in S11, where the mechanisms of supercooled raindrops directly freezing to graupel were switched off. There was no time to produce graupel by other means, i.e. by ice particle growing by diffusion and then by riming before the cloud dissipated, and there were insufficient cloud drops for the operation of the HM process. These findings in S11 are consistent with the modelling studies of Phillips *et al.* (2001).

To investigate which mechanism is more important in the production of graupel through freezing of raindrops, two sensitivity tests S12 and S13 were performed. In S12 the mechanism of immersion freezing was switched off. The results in Table 4 show that there were no large differences between S12 and the reference run regarding the maximum concentration of graupel, the ice concentration, the HM production rate, the ice nucleation rate of deposition/condensation freezing, and the graupel production rate by collection processes. This suggests that the mechanism of immersion freezing of raindrops as defined in the model is not as important as the other mechanism of raindrops freezing by collecting ice in the production of graupel. Phillips

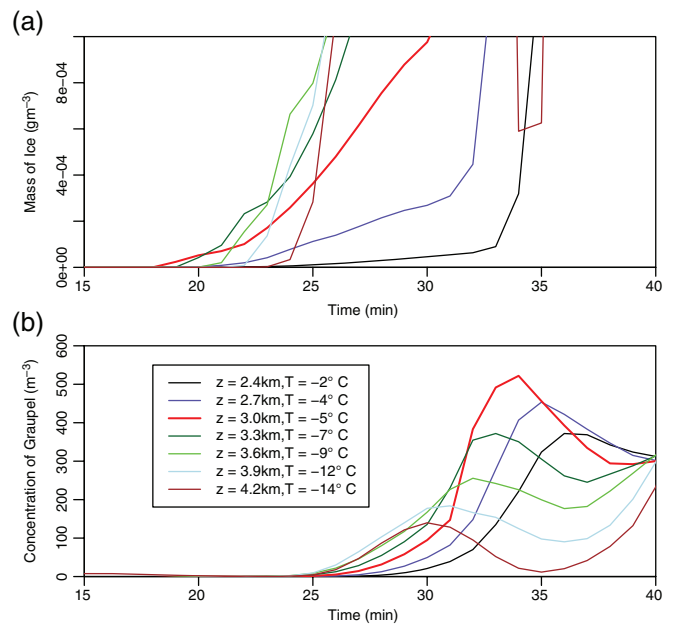


Figure 4. Evolution of (a) maximum ice mass and (b) concentration of graupel at $z = 2.4$ to 4.2 km for S10.

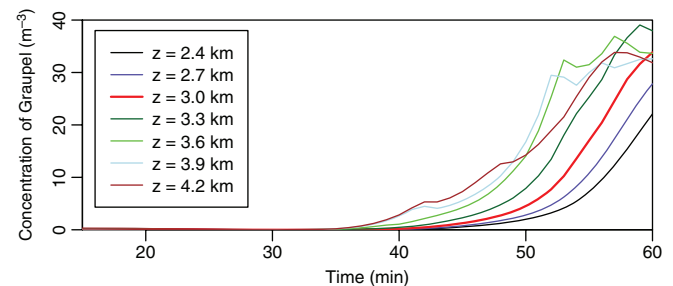


Figure 5. Evolution of maximum concentration of graupel at $z = 2.4$ to 4.2 km for S11.

et al. (2001) also found that graupel particles are produced by raindrops freezing upon impact with primary ice crystals.

S13 is the sensitivity simulation where the mechanism of deposition/condensation freezing was switched off. Figure 6 shows the evolution of ice mass and graupel concentration at altitudes from $z \approx 2.4$ to 4.2 km. The ice particles first formed at $z \approx 4.2$ km ($T \approx -15^\circ\text{C}$) at 25 min due to immersion freezing, rather than at 3 km ($T \approx -5^\circ\text{C}$) at 17 min in the reference run. The ice particles then grew by diffusion so there was an increase in ice mass reaching 0.001 gm^{-3} at about 33 min, 8 min later than in the reference run (Figure 4(a)). The delayed development of ice particles led to the delayed development of graupel. From Figure 6(b), it can be seen that graupel first formed at $z \approx 4.2$ km at 25 min, but then the concentration of graupel increased slowly, until ice mass had a rapid growth. The concentration of graupel at $z \approx 3$ km reached 0.1 L^{-1} at 33 min, 3 min later than in the reference run (Figure 4(b)). The delayed and suppressed development of graupel led to delayed and suppressed development of secondary ice in this run.

From Table 4, it can be seen that the maximum concentration of graupel reduced from 230.2 m^{-3} in the reference run to 136.7 m^{-3} in S13. The maximum ice multiplication rate also reduced significantly from 1075 to $428.6 \text{ m}^{-3} \text{ s}^{-1}$ and the maximum occurred about 5 min later than in S10. Therefore, the maximum concentration of ice decreased from 171 L^{-1} in S10 to 17.85 L^{-1} in S13. The results of the sensitivity simulations S12 and S13 showed that the mechanism of raindrops freezing upon impact with ice crystals was more important than the mechanism of immersion freezing of raindrops for the production of graupel. In addition, the first ice produced by deposition/condensation freezing was more important to the HM process than the ice

Table 4. Maximum concentrations of ice crystals (N_i) and graupel particles (N_g), ice production rates of multiplication (S_{nimul}), immersion freezing (S_{nifre}), and deposition/condensation freezing (S_{nidep}), and graupel production rates by immersion freezing (S_{ngfre}) and collection process (S_{ngcol}) for the simulations shown in Table 3. N_g is the maximum before the S_{nimul} is reached.

Run	N_i (L^{-1})	S_{nimul} ($m^{-3} s^{-1}$)	S_{nifre} ($m^{-3} s^{-1}$)	S_{nidep} ($m^{-3} s^{-1}$)	N_g (m^{-3})	S_{ngfre} ($m^{-3} s^{-1}$)	S_{ngcol} ($m^{-3} s^{-1}$)
S10	171.000	1075 (30)	0.811 (30)	102.9 (30)	230.20	0.4341 (30)	1.967 (30)
S11	46.920	0.0002 (45)	45.33 (40)	472 (40)	42.37	0	0.226 (50)
S12	179.100	1143 (30)	0	102.5 (30)	229.80	0	1.958 (30)
S13	17.850	428.6 (35)	4.858 (35)	0	136.70	0.7457 (35)	2.144 (35)
S14	22.710	356 (35)	0	0.4777 (35)	152.80	0	1.306 (35)
S15	0.470	1.9 (50)	0	0.1782 (40)	19.90	0	0.063 (40)
S20	2.198	9.4 (50)	0.0354 (40)	45.84 (40)	38.92	0.0047 (45)	0.253 (45)
S21	8.290	131.3 (45)	0.0446 (40)	96.68 (45)	92.95	0.0315 (40)	0.774 (45)
S22	8.157	48.9 (35)	0.0870 (30)	59.27 (25)	115.30	0.0896 (30)	0.938 (30)
S23	8.194	47.9 (35)	0.0845 (30)	133.9 (20)	173.90	0.0858 (30)	1.468 (30)

The timings (in min) of these values are shown in brackets.

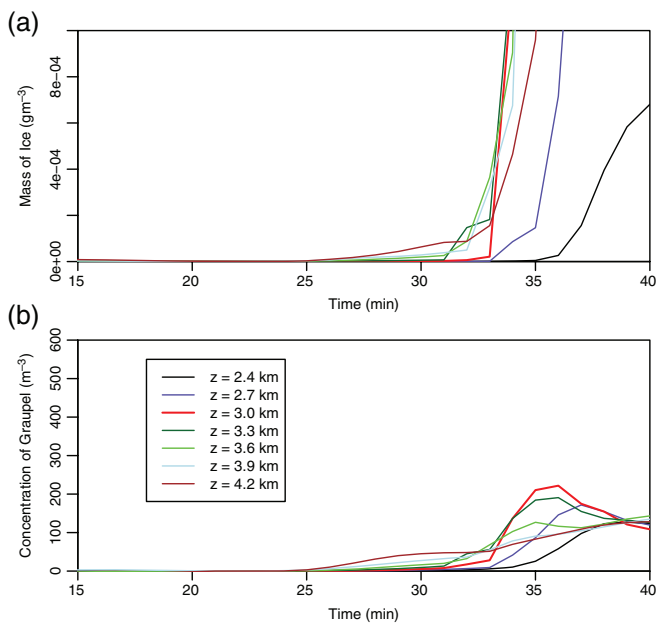


Figure 6. Evolution of (a) maximum ice mass and (b) concentration of graupel at $z = 2.4$ to 4.2 km for S13.

produced by immersion freezing for the cumulus cloud with moderate top temperatures ($T > -20$ °C), at least for the ice nucleation parametrizations used herein.

An important question is what concentration of primary ice is sufficient to allow an effective secondary ice production of the HM process in these clouds. Sensitivity tests S14 and S15 were made to address this question. The equation for the deposition/condensation freezing scheme includes a multiplying factor of 0.005 and 0.0005 respectively, and the immersion freezing was switched off. From Table 4, it can be seen that the maximum ice multiplication rate and ice concentration were $356 m^{-3} s^{-1}$ and $22.71 L^{-1}$ respectively in S14, but were only $1.87 m^{-3} s^{-1}$ and $0.47 L^{-1}$ respectively in S15. The reason for the relatively ineffective operation of the HM process in S15 can be explained in Figure 7.

It is evident that the formation of the first ice was more suppressed in S15 than in S14 (Figure 7(a)), leading to less graupel being produced (Figure 7(b)) since, as mentioned above, graupel was mainly produced by supercooled raindrops freezing upon impact with ice. By the time a maximum concentration of graupel ($0.02 L^{-1}$) was produced at 42 min in S15 (Figure 7(b)), the concentration of cloud drops at 3 km was only $13 cm^{-3}$ (Figure 7(c)). However, in S14 there was a significant amount of graupel (greater than $0.1 L^{-1}$) at 36 min where there were still sufficient numbers of cloud drops available ($68 cm^{-3}$) and thus the HM process was much more effective. Therefore, the

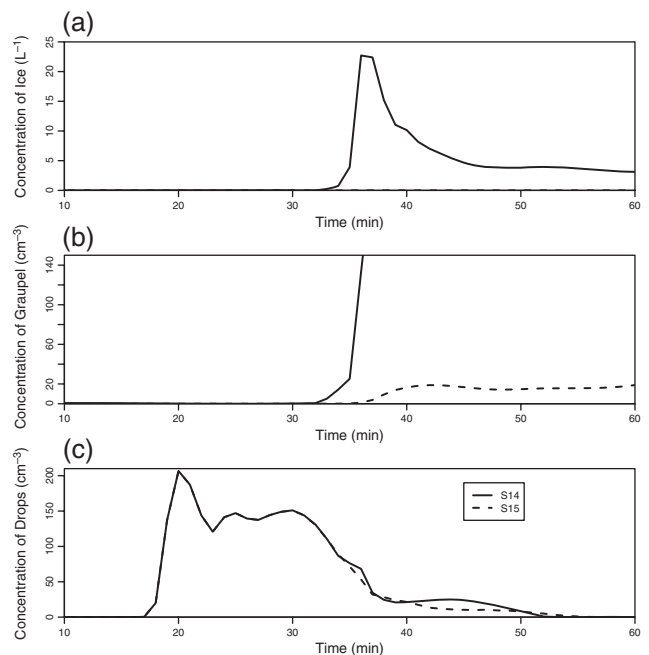


Figure 7. Time evolutions of maximum concentrations of (a) ice, (b) graupel, and (c) drops at $z = 3$ km ($T \approx -5$ °C). The solid and dashed lines represent S14 and S15, respectively.

concentration of the first ice can be as little as 0.5% of the original amount of deposition/condensation freezing nuclei, which is about $0.01 L^{-1}$, for the HM process to produce a significant concentration of secondary ice particles in this particular cloud. Figure 7 clearly shows that there is a major change between 0.01 and $0.001 L^{-1}$. This result is in agreement with the inference drawn by Crawford *et al.* (2012) from the observations.

4.3. Reference Run S20: the 13 July 2005 cloud

The reference run of the 13 July cloud was also performed for 1 h, by using the initial conditions mentioned in section 3.2 and in Table 3. It is important to point out that the initial aerosol background conditions on 13 July were characterized with significantly larger total loading and more small and large aerosols, but fewer giant aerosols than on 18 May (Table 2).

Figure 8 shows the sequence of spatial distribution of the wind field and concentrations of drops, ice and graupel particles from 25 to 50 min into the simulation, at 5 min intervals.

Before 35 min (Figures 8(a)–(c)) the cloud was young and growing. A small concentration of ice particles ($1.3 L^{-1}$ in maximum) formed near cloud top at 35 min due to deposition/condensation freezing. The maximum vertical velocity was $11.5 m s^{-1}$ and the maximum concentration of cloud drops

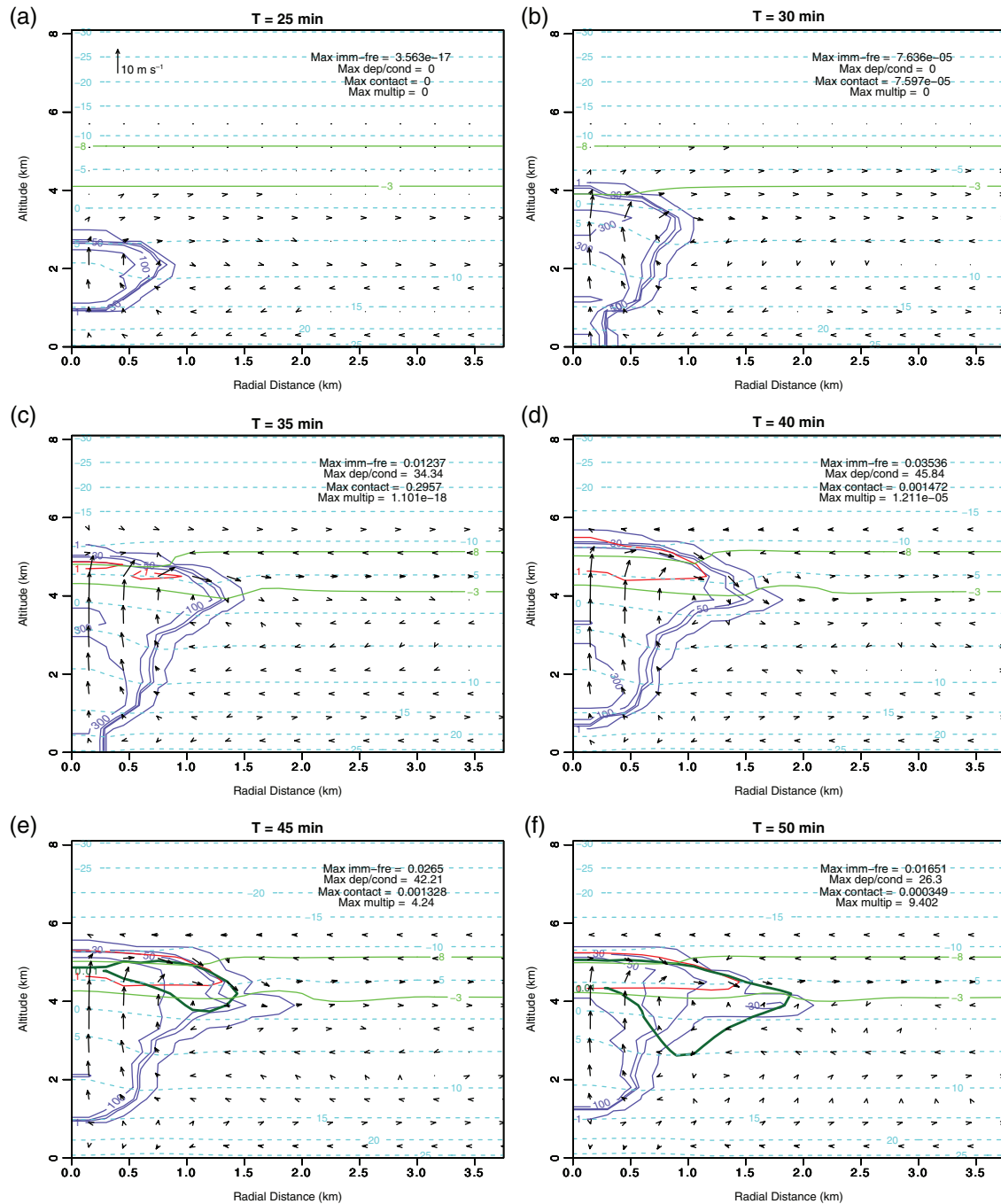


Figure 8. As Figure 2, but for run S20 at time steps (a) 25 min, (b) 30 min, (c) 35 min, (d) 40 min, (e) 45 min and (f) 50 min.

was 256 cm^{-3} at 3.9 km. The maximum concentration of large droplets ($d > 24 \mu\text{m}$) was 59 cm^{-3} at 3.9 km, a little greater than that of the small droplets ($d < 13 \mu\text{m}$) (56 cm^{-3}). The cloud grew until 40 min when the cloud top reached a temperature $T \approx -12^\circ\text{C}$ (Figure 8(d)).

The cloud had become mature by 45 min (Figure 8(e)). The maximum vertical velocity had reduced to 10.7 m s^{-1} . The maximum concentration of ice and graupel particles had increased to 1.9 L^{-1} and 22.6 m^{-3} , respectively. The maximum concentration of large droplets at 5.1 km had increased to 75 cm^{-3} , much higher than that of small droplets (10 cm^{-3}). The cloud had started to decay at 50 min (Figure 8(f)). From Table 1 and Figure 8 it can be seen that the general features of the simulated cloud were close to the observations, such as the maximum vertical velocity (11.5 m s^{-1}), the concentration of droplets ($200\text{--}300 \text{ cm}^{-3}$), the low concentrations of ice and graupel particles, and the change in the concentrations of large and small droplets with the cloud development.

The maximum ice production rate due to the HM process was only $9.402 \text{ m}^{-3} \text{ s}^{-1}$ (Figure 8(f)), much smaller than $1075 \text{ m}^{-3} \text{ s}^{-1}$

in the 18 May cloud, showing that the HM process did not operate effectively in the 13 July cloud. The reason for this is now discussed. The freezing of supercooled raindrops by interacting with ice crystals was the main mechanism for the formation of graupel particles, similar to the 18 May cloud. Figure 9 shows the time evolution of the concentration of cloud drops, raindrops and graupel particles and ice mass and concentration at $z \approx 4.5 \text{ km}$ ($T \approx -5^\circ\text{C}$) for the reference run (S20) and other sensitivity runs discussed below. The solid black lines are the results of the reference run. The formation of graupel occurred after the increase in ice mass (Figure 9(d)), which was similar to the 18 May case. However, the formation of raindrops and thus graupel occurred later in the 13 July cloud than in the 18 May cloud and the concentrations were lower. The maximum concentrations of raindrops and graupel at $T \approx -5^\circ\text{C}$ were 0.24 L^{-1} (Figure 9(c)) and 31 m^{-3} (Figure 9(d)), respectively, compared to values of 0.56 L^{-1} and 520 m^{-3} in 18 May reference simulation cloud (Figures 3 and 4).

The low concentration of raindrops and hence graupel particles produced in the 13 July cloud was the main cause of the

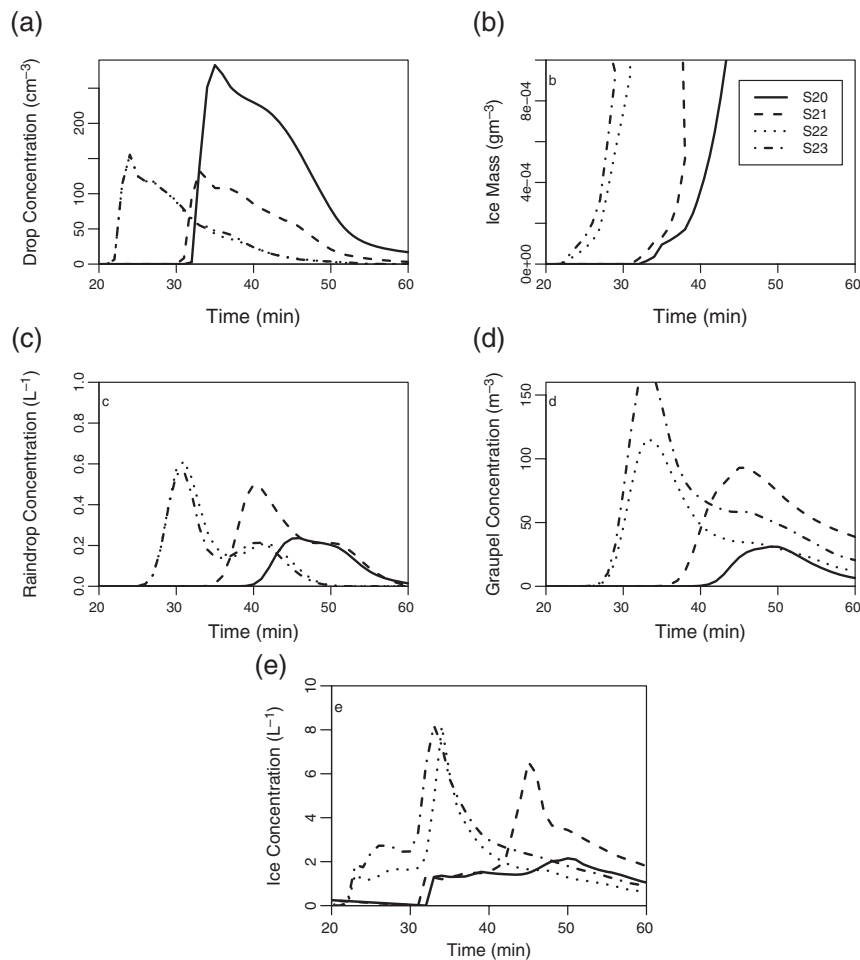


Figure 9. For runs S20, S21, S22 and S23, time evolution of the maximum concentration of (a) cloud drops, (c) raindrops and (d) graupel particles, and (b) ice mass and (e) ice concentration at $z \approx 4.5$ km ($T \approx -5^\circ\text{C}$).

ineffective operation of the HM process. It is expected in the 13 July case that the high aerosol loading was responsible for the more numerous, but smaller, drops and low concentration of supercooled raindrops. Sensitivity studies were performed in order to investigate if other factors might have contributed, such as the initial aerosol background conditions, the strength of the initial warm bubble, and the temperatures at cloud-base and cloud-top levels. The results of these simulations are discussed in the next section.

4.4. Sensitivity simulations S21 to S23: the 13 July 2005 cloud

The configuration of S21 was the same as that of the reference run S20, but the initial aerosol background conditions of the 18 May case were used (Table 2). The dashed lines in Figure 9 are from the results of S21. There was a lower concentration of cloud drops, as expected (Figure 9(a)). There was a greater concentration of raindrops and they formed earlier (Figure 9(c)). The first ice particles also formed a little earlier and grew faster in S21 than in S20 (Figure 9(b)) due to higher supersaturation with respect to ice, since the supersaturation with respect to water was higher as a result of lower concentration of cloud drops in S21 than in S20 (Figure 9(a)). Therefore, graupel was produced earlier and there was a greater concentration in S21 (Figure 9(d)). The effect of this on the HM process is shown in Table 4. The ice production rate of the HM process was enhanced to a maximum of $131.3 \text{ m}^{-3} \text{ s}^{-1}$ and the maximum concentration of ice increased to 8.2 L^{-1} . Therefore, the more polluted nature of the 13 July cloud may have contributed to the ineffective operation of the HM process. However, the ice multiplication rate in S21 is still much lower than that in the reference run of the 18 May case.

A strong thermal bubble was used in run S22 in order to test the influence of the strength on the HM process. The results are

shown in Figure 9. The cloud occurred about 9 min earlier in S22 than in S20 (Figure 9(a)) and the concentration of raindrops (and hence graupel) was a little greater. However, the maximum ice concentration was still low (8.157 L^{-1}) and the ice production rate of the HM process was even lower ($48.92 \text{ m}^{-3} \text{ s}^{-1}$) than that in S21 (Table 4). In addition, the maximum ice production rate of deposition/condensation freezing was only $59.27 \text{ m}^{-3} \text{ s}^{-1}$, which is about half of the corresponding values of S21 and S10. Therefore, the stronger thermal bubble did not have an important influence on the HM process in the 13 July case.

Considering that the cloud-top temperature of the 13 July cloud (-12°C) was significantly greater than that of the 18 May cloud (-18°C), so there was less primary ice, the sensitivity test S23 was performed with an artificially enhanced Meyers scheme (Meyers *et al.*, 1992), where the formula of deposition/condensation freezing included a multiplication factor of 2, and there was no restriction of $T < -5^\circ\text{C}$ required for ice particles to be produced. The results are shown in Figure 9. It is clearly seen that the concentration of graupel is greater in run S23 as a result of the enhanced production of the primary ice particles. The graupel was formed by collisions between supercooled raindrops and ice crystals. The increase in the concentration of graupel in response to increasing the concentration of ice crystals activated by primary nucleation by a factor of 2 is therefore further evidence that the above mechanism of the production of graupel from supercooled raindrops is the main mechanism. The maximum concentration of graupel increased from 115.3 m^{-3} in S22 to 173.9 m^{-3} in S23 (Table 4). This value was closest to that in S14 (152.8 m^{-3}) among the 18 May simulations. However, the maximum concentration of ice particles and the ice production rate of the HM process in S23 were both significantly lower than those values in S14.

Figure 10 illustrates the reason for the less effective operation of the HM process in S23 than in S14. It shows the radial distribution of the concentration of large and small cloud droplets

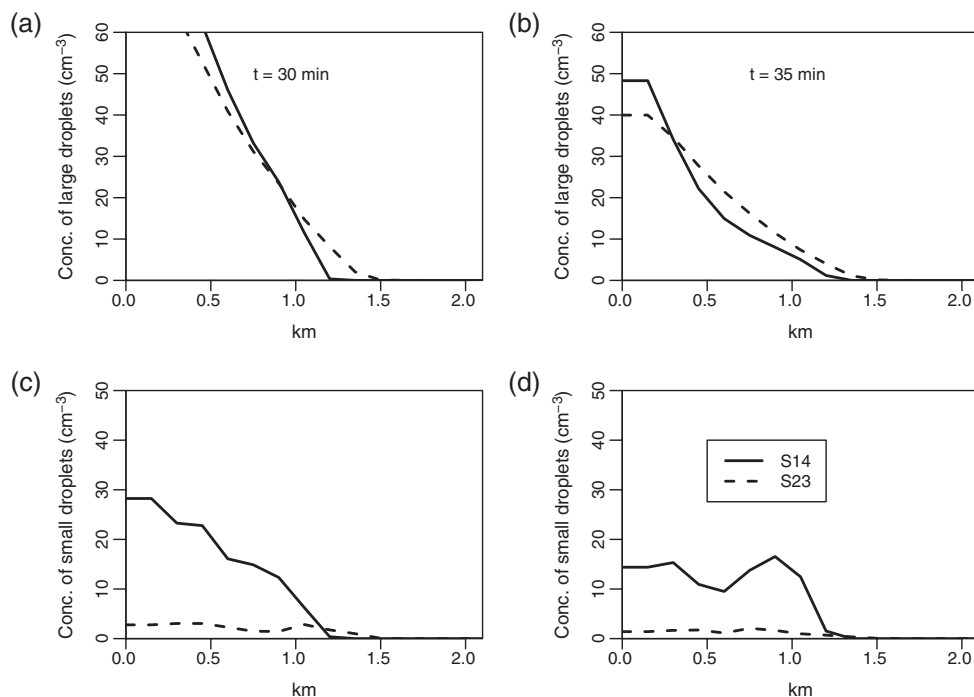


Figure 10. For runs S14 and S23, radial distribution of the concentration of (a, b) large and (c, d) small cloud droplets at the $T \approx -5^\circ\text{C}$ level at (a, c) 30 min and (b, d) 35 min.

at $T \approx -5^\circ\text{C}$ at 30 and 35 min, when the HM process was operating. It is apparent that the concentration of large droplets in S23 was similar to that in S14, but the concentration of small droplets in S23 was much lower than that in S14. The maximum concentration of small droplets in S23 was only 3 and 2 cm^{-3} at 30 and 35 min, respectively, whereas it was 28 and 17 cm^{-3} in S14 at 30 and 35 min, respectively. The concentration of small droplets in both of the cases decreased as the cloud aged, which is in agreement with the observations (Huang, 2014, Chapter 5). The secondary ice production rate of the HM process in S23 was significantly lower, since there were fewer small droplets available than in S14. This difference may be caused by the difference in the cloud-base temperature and thus the depth from the base to -5°C level, provided the aerosol properties were the same, or a difference in the dynamics and amount of entrainment. The cloud-base temperature in S23 was about 15°C (Figure 8), which is significantly greater than 10°C (Figure 2) in S14. The greater depth from the cloud base to the -5°C level in S23 allowed more droplets to grow into larger ones in the updraught. Therefore, the concentration of small droplets at the -5°C level was lower in the greater depth case than in a thinner situation. In addition to this, the concentration of small droplets generally decreases with the increase of the distance from cloud base.

5. Summary and conclusions

Modelling analysis is presented in this article of the production of ice and precipitation for two observed convective cloud systems studied in the south of England and Wales as part of the ICEPIC project. The cases were on 18 May 2006 in Devon and 13 July 2005 in Wales. The clouds grew in different thermodynamic conditions in environments that contained significantly different aerosol concentrations.

The aircraft made passes through the 18 May cloud at temperatures from -1 to -7.9°C as the cloud tops ascended. Supercooled raindrops were observed when the concentration of ice particles was only a few per litre. High concentrations of ice particles (110L^{-1}) were subsequently observed during the later penetrations and the conditions were conducive for the HM process. The agreement between the simulation of the single-thermal cloud and the observations suggested that the HM

process was responsible for the observed high concentration of ice particles.

Sensitivity simulations of the cloud were conducted to investigate the role of supercooled raindrops in the development of ice and in the operation of the HM process. The sensitivity simulations showed that the fast production of graupel by freezing of supercooled raindrops was crucial to the activation of the HM process. When the mechanisms of raindrops freezing to graupel were switched off in this cloud, the production of graupel was much delayed and suppressed and thus the HM process did not occur. Furthermore, in the two mechanisms of the production of graupel, the freezing of raindrops through collisional collection with ice particles was more important than through immersion freezing. In addition, the production of graupel was more sensitive to the primary ice produced by deposition/condensation freezing than by immersion freezing for the case with a moderately low cloud top temperature (e.g. $T_{\text{ct}} > -20^\circ\text{C}$). A concentration of only approximately 0.01L^{-1} generated by the primary ice process was sufficient in the model to allow the HM process to become significant, as long as there was a large enough concentration of cloud droplets (small and large) available when a significant number of graupel particles developed in the HM temperature zone.

The modelled results indicate the requirement of a low concentration of primary ice particles for the HM process to initiate which can result from the deposition/condensation freezing. Recently, Hiron and Flossmann (2015) made an assessment of the deposition, condensation, contact, immersion and homogeneous freezing schemes. They found that deposition freezing starts first at higher temperatures, followed by the condensation freezing, and the immersion freezing takes over at lower temperatures. Our modelling results of the initial freezing modes are consistent with the results of Hiron and Flossmann (2015). However, there is uncertainty about the initial formation of primary ice particles since other freezing modes might contribute to the initial ice formation. For example, biogenic ice nucleating particles can nucleate ice at higher temperatures than soot or dust (Murray *et al.*, 2012). It is also worth noting that there is debate about the extent to which the deposition and condensation freezing modes exist (e.g. Marcolli, 2014; Wex *et al.*, 2014; Vali *et al.*, 2015). Also, it has been found that even dust particles, which are often assumed to be insoluble, can act as CCN

through adsorption of water or through soluble material being present (Karydis *et al.*, 2011), which would prevent deposition ice nucleation on these in atmospheric mixed phase clouds.

Three aircraft passes were made in the second case (13 July 2005) at temperatures from -2.5 to -6.6 °C in a cloud that developed over Wales. Supercooled raindrops were observed, but in much lower concentrations than in the 18 May clouds. The concentration of cloud drops was high as a result of the high aerosol concentrations and the concentration of ice particles was low. The simulation of the 13 July case indicated that the HM process did not operate effectively in this cloud mainly because of the low concentration of supercooled raindrops and hence graupel particles.

Sensitivity simulations suggested that the relatively greater number of aerosols and higher cloud-base and cloud-top temperatures also contributed to the ineffective operation of the HM process and thus to the observed low concentration of ice particles in the 13 July cloud. The aerosol properties had an impact on the production of raindrops and graupel particles and thus on the HM process. The cloud-top temperature had an impact on the concentration of the primary ice and then on the production of graupel. Mossop (1978b) attempted to separate cloud conditions which are favourable for the HM process to take place from those which are unfavourable. He suggested that the cloud-base temperature and the cloud drop concentration are the main factors because they govern the concentration of drops greater than $25\ \mu\text{m}$ in the HM zone. The studies of the two cases here indicated that the presence of supercooled raindrops was necessary to the operation of the HM process in the model, but not sufficient. The simulations of the 13 July cloud showed that the sufficient concentration of small droplets ($d < 13\ \mu\text{m}$) in the HM zone was another essential element, which can also be affected by the cloud-base temperature. Therefore, the operation of the HM process was not only affected by the microphysics of the cloud but also the macrophysics.

It is well known that supercooled raindrops play an important role in the ice process (e.g. Koenig, 1977; Lamb *et al.*, 1981; Phillips *et al.*, 2001). The model results herein are consistent with those of Chisnell and Latham (1976) and Blyth and Latham (1997).

There remains uncertainty about the interaction of dynamics and the HM process in the observed clouds. For example, it is unclear if there were multiple thermals. So, although the model results suggest that the HM process is responsible for the observed high concentrations of ice particles, it is not possible to provide a full explanation for the development. It should be pointed out that the production of graupel through diffusional growth of ice followed by riming, which is a much slower process, may be still possible for an efficient operation of the HM process if there is sufficient time. One possibility is that the convective clouds possess a multi-thermal structure as observed over New Mexico (Blyth and Latham, 1997). Graupel particles produced well above the HM zone may then be incorporated into the new thermal and reach the HM zone.

This article has studied the cloud conditions thought to be important for the HM process with a model that represents the process with parametrized equations. It is claimed that there is a 'strong suggestion' that the HM process is responsible for the production of ice in the 18 May case because the model produces significant ice by the HM process and little ice in the other for physical reasons that match the conditions observed in the clouds. However, Knight (2012) argued convincingly that the rupturing of the frozen shell surrounding the liquid in the larger droplets on the surface of the rimed particles to produce splinters requires a degree of violence that is highly unlikely to occur. He presents results of careful laboratory studies performed at a temperature of -5 °C which show the possibility of a different ice multiplication mechanism that does not involve riming. Recently Lawson *et al.* (2015) showed that the fracturing of raindrops as observed by Leisner *et al.* (2014) in the laboratory might lead to a production of secondary ice as they freeze. While the observations in the current work suggest that the total amount

of riming is important, there is no information at all on how the ice splinters are produced. Refined laboratory experiments, advanced measurement techniques, and more field campaigns will enable us to understand the secondary ice production better in the future.

Acknowledgements

We would like to thank the pilots and staff of the FAAM BAe-146 aircraft for making the aircraft measurements possible, and instrument scientists of the National Centre for Atmospheric Science (NCAS) Atmospheric Measuring Facility (AMF) for running instruments on the aircraft and on the ground. This work was funded by the Natural Environmental Research Council (NERC) with grant number NER/A/S/2002/00956.

References

- Bigg EK. 1953. The formation of atmospheric ice crystals by the freezing of droplets. *Q. J. R. Meteorol. Soc.* **79**: 510–519.
- Blyth AM, Latham J. 1993. Development of ice and precipitation in New Mexican summertime cumulus cloud. *Q. J. R. Meteorol. Soc.* **119**: 91–120.
- Blyth AM, Latham J. 1997. A multi-thermal model of cumulus glaciation via the Hallett-Mossop process. *Q. J. R. Meteorol. Soc.* **123**: 1185–1198.
- Blyth AM, Benestad R, Krehbiel P, Latham J. 1997. Observations of supercooled raindrops in New Mexico summertime cumuli. *J. Atmos. Sci.* **54**: 569–575.
- Blyth AM, Lowenstein JH, Huang Y, Cui Z, Davies S, Carslaw KS. 2012. The production of warm rain in shallow maritime cumulus clouds. *Q. J. R. Meteorol. Soc.* **139**: 20–31.
- Bower K, Moss S, Johnson D, Choulaton T, Latham J, Brown P, Blyth AM, Cardwell J. 1996. A parametrization of the ice water content observed in frontal and convective clouds. *Q. J. R. Meteorol. Soc.* **122**: 1815–1844.
- Brenguier JL, Bourriane T, Coelho AD, Isbert J, Peytavi R, Trevarin D, Weschler P. 1998. Improvements of droplet size distribution measurements with the Fast-FSSP (Forward Scattering Spectrometer Probe). *J. Atmos. Oceanic Technol.* **15**: 1077–1090.
- Brangi V, Knupp K, Detwiler A, Liu L, Caylor IJ, Black RA. 1997. Evolution of a Florida thunderstorm during the convection and precipitation/electrification experiment: The case of 9 August 1991. *Mon. Weather Rev.* **125**: 2131–2160.
- Caylor I, Illingworth A. 1987. Radar observations and modelling of warm rain initiation. *Q. J. R. Meteorol. Soc.* **113**: 1171–1191.
- Chisnell RF, Latham J. 1976. Ice particle multiplication in cumulus clouds. *Q. J. R. Meteorol. Soc.* **102**: 133–156.
- Cotton WR, Tripoli GJ, Rauber RM, Mulvihill E. 1986. Numerical simulation of the effects of varying ice crystal nucleation rates and aggregation processes on orographic snowfall. *J. Clim. Appl. Meteorol.* **25**: 1658–1680.
- Crawford I, Bower KN, Choulaton TW, Dearden C, Crosier J, Westbrook C, Capes G, Coe H, Connolly PJ, Dorsey JR, Gallagher MW, Williams P, Trembath J, Cui Z, Blyth AM. 2012. Ice formation and development in aged, wintertime cumulus over the UK: Observations and modelling. *Atmos. Chem. Phys.* **12**: 4963–4985, doi: 10.5194/acp-12-4963-2012.
- Crosier J, Bower KN, Choulaton TW, Westbrook CD, Connolly PJ, Cui ZQ, Crawford IP, Capes GL, Coe H, Dorsey JR, Williams PI, Illingworth AJ, Gallagher MW, Blyth AM. 2011. Observations of ice multiplication in a weakly convective cell embedded in supercooled mid-level stratus. *Atmos. Chem. Phys.* **11**: 257–273, doi: 10.5194/acp-11-257-2011.
- Cui Z, Carslaw KS. 2006. Enhanced vertical transport efficiency of aerosol in convective clouds due to increases in tropospheric aerosol abundance. *J. Geophys. Res.* **111**: D15212, doi: 10.1029/2005JD006781.
- Cui Z, Carslaw K, Yin Y, Davies S. 2006. A numerical study of aerosol effects on the dynamics and microphysics of a deep convective cloud in a continental environment. *J. Geophys. Res.* **111**: D05201, doi: 10.1029/2005JD005981.
- Cui Z, Davies S, Carslaw KS, Blyth AM. 2011. The response of precipitation to aerosol through riming and melting in deep convective clouds. *Atmos. Chem. Phys.* **11**: 3495–3510, doi: 10.5194/acp-11-3495-2011.
- Field P, Heymsfield A. 2015. Importance of snow to global precipitation. *Geophys. Res. Lett.* **42**: 9512–9520, doi: 10.1002/2015GL065497.
- Hallett J, Mossop S. 1974. Production of secondary ice crystals during the riming process. *Nature* **249**: 26–28.
- Harris-Hobbs R, Cooper W. 1987. Field evidence supporting quantitative predictions of secondary ice production rate. *J. Atmos. Sci.* **44**: 1071–1082.
- Hiron T, Flossmann AI. 2015. A study of the role of the parameterization of heterogeneous ice nucleation for the modeling of microphysics and precipitation of a convective cloud. *J. Atmos. Sci.* **72**: 3322–3339, doi: 10.1175/JAS-D-15-0026.1.
- Hobbs PV, Rangno A. 1985. Ice particle concentrations in clouds. *J. Atmos. Sci.* **42**: 2523–2549.
- Huang Y. 2014. 'The formation and development of ice and precipitation in convective clouds', PhDthesis. University of Leeds: UK.

- Huang Y, Blyth AM, Brown PRA, Choullarton TW, Connolly P, Gadian AM, Jones H, Latham J, Cui Z, Carslaw K. 2008. The development of ice in a cumulus cloud over southwest England. *New J. Phys.* **10**: 105021, doi: 10.1088/1367-2630/10/10/105021.
- Huang Y, Blyth AM, Brown PRA, Cotton R, Crosier J, Bower KN, Gallagher MW, Jones H, Gadian AM, Choullarton TW, Cardwell J, Coe H, Mobbs SD, Hagen M. 2011. Development of ice particles in convective clouds observed over the Black Forest mountains during COPS. *Q. J. R. Meteorol. Soc.* **137**: 275–286. doi: 10.1002/qj.749.
- Jensen JB, Granek H. 2002. Optoelectronic simulation of the PMS 260X Optical Array Probe and application to drizzle in a marine stratocumulus. *J. Atmos. Oceanic Technol.* **19**: 376–389.
- Karydis VA, Kumar P, Barahona D, Sokolik IN, Nenes A. 2011. On the effect of dust particles on global cloud condensation nuclei and cloud droplet number. *J. Geophys. Res.* **116**: D23204, doi: 10.1029/2011JD016283.
- Knight CA. 2012. Ice growth from the vapor at -5° C. *J. Atmos. Sci.* **69**: 2031–2040.
- Knollenberg RG. 1970. The optical array: An alternative to extinction and scattering for particle size measurement. *J. Appl. Meteorol.* **9**: 86–103.
- Koenig LR. 1977. The rime-splintering hypothesis of cumulus glaciation examined using a field-of-flow cloud model. *Q. J. R. Meteorol. Soc.* **103**: 585–606.
- Korolev AV. 2007. Reconstruction of the sizes of spherical particles from their shadow images. Part I: Theoretical considerations. *J. Atmos. Oceanic Technol.* **24**: 376–389.
- Korolev AV, McFarquhar G, Lawson P, Gayet J-F, Kraemer M, Heymsfield A, Rogers D, Twohy C, Stetzer O. 2010. 'The effect of ice bouncing and shattering on the performance of airborne cloud microphysical instrumentation'. In *AMS Conference Proceedings, July 2010, Portland, OR*.
- Lamb D, Hallett J, Sax RI. 1981. Mechanistic limitations to the release of latent heat during the natural and artificial glaciation of deep convective clouds. *Q. J. R. Meteorol. Soc.* **107**: 935–954.
- Lawson RP, Baker BA, Schmitt CG, Jensen TL. 2001. An overview of microphysical properties of Arctic clouds observed in May and July 1998 during FIRE ACE. *J. Geophys. Res. Atmos.* **106**: 14989–15014.
- Lawson RP, Woods S, Morrison H. 2015. The microphysics of ice and precipitation development in tropical cumulus clouds. *J. Atmos. Sci.* **72**: 2429–2445, doi: 10.1175/JAS-D-14-0274.1.
- Leisner T, Pander T, Handmann P, Kiselev A. 2014. 'Secondary ice processes upon heterogeneous freezing of cloud droplets'. In *it14th Conference on Cloud Physics and Atmospheric Radiation*. American Meteorological Society: Boston, MA.
- Lew JK, Pruppacher HR. 1983. A theoretical determination of the capture efficiency of small columnar ice crystals by large cloud drops. *J. Atmos. Sci.* **40**: 139–145.
- Marcolli C. 2014. Deposition nucleation viewed as homogeneous or immersion freezing in pores and cavities. *Atmos. Chem. Phys.* **14**: 2071–2104.
- Meyers M, DeMott PJ, Cotton W. 1992. New primary ice-nucleation parameterizations in an explicit cloud mode. *J. Appl. Meteorol.* **31**: 708–721.
- Mossop S. 1978a. The influence of drop size distribution on the production of secondary ice particle during graupel growth. *Q. J. R. Meteorol. Soc.* **104**: 323–330.
- Mossop S. 1978b. Some factors governing ice particle multiplication in cumulus clouds. *J. Atmos. Sci.* **35**: 2033–2037.
- Mossop S. 1985. The origin and concentration of ice crystals in clouds. *Bull. Am. Meteorol. Soc.* **66**: 264–273.
- Mossop S, Hallett J. 1974. Ice crystal concentration in cumulus clouds: Influence of the drop spectrum. *Science* **186**: 632–634.
- Mossop S, Cottis R, Bartlett B. 1972. Ice crystal concentrations in cumulus and stratocumulus clouds. *Q. J. R. Meteorol. Soc.* **98**: 105–123.
- Murray BJ, O'Sullivan D, Atkinson JD, Webb ME. 2012. Ice nucleation by particles immersed in supercooled cloud droplets. *Chem. Soc. Rev.* **41**: 6519–6554.
- Phillips V, Blyth AM, Brown P, Choullarton TW, Latham J. 2001. The glaciation of a cumulus cloud over New Mexico. *Q. J. R. Meteorol. Soc.* **127**: 1513–1534.
- Reisin T, Levin Z, Tzivion S. 1996. Rain production in convective clouds as simulated in an axisymmetric model with detailed microphysics. Part I: Description of the model. *J. Atmos. Sci.* **53**: 497–520.
- Strapp J, Leaitch W, Liu P. 1992. Hydrated and dried aerosol-size distribution measurements from the particle measuring systems FSSP-300 probe and the deiced PSASP-100X probe. *J. Atmos. Oceanic Technol.* **9**: 548–555.
- Strapp J, Oldenburg J, Ide R, Lilie L, Bacic S, Vukovic Z, Oleskiw M, Miller D, Emery E, Leone G. 2003. Wind tunnel measurements of the response of hot-wire liquid water content instruments to large droplets. *J. Atmos. Oceanic Technol.* **20**: 791–806.
- Sun J, Ariya PA, Leighton HG, Yau MK. 2012. Modeling study of ice formation in warm-based precipitating shallow cumulus clouds. *J. Atmos. Sci.* **69**: 3315–3335.
- Tzivion S, Feingold G, Levin Z. 1987. An efficient numerical solution to the stochastic collection equation. *J. Atmos. Sci.* **44**: 3139–3149.
- Vali G, DeMott PJ, Moehler O, Whale TF. 2015. Technical note: A proposal for ice nucleation terminology. *Atmos. Chem. Phys.* **15**: 10263–10270.
- Wex H, DeMott PJ, Tobo Y, Hartmann S, Rösch M, Clauss T, Tomsche L, Niedermeier D, Stratmann F. 2014. Kaolinite particles as ice nuclei: Learning from the use of different kaolinite samples and different coatings. *Atmos. Chem. Phys.* **14**: 5529–5546.
- Yin Y, Carslaw K, Feingold G. 2005. Vertical transport and processing of aerosols in a mixed-phase convective cloud and the feedback on cloud development. *Q. J. R. Meteorol. Soc.* **131**: 221–245.